

Thermo-optic Coefficient of Electrochemically Etched Porous Silicon

Lorenzo P. Lopez Jr.^{1,*}, Arvin I. Mabilangan², Maria Angela B. Faustino¹, Niel Gabriel E. Saplagio¹, Arnel A. Salvador², and Armando S. Somintac^{1,2}

¹ Material Science and Engineering Program, University of the Philippines, Diliman, Quezon City

² Condensed Matter Physics Laboratory, National Institute of Physics, University of the Philippines, Diliman, Quezon City

*E-mail: llopez@nip.upd.edu.ph

Received: 1 July 2014 / Accepted: 15 September 2014 / Published: 28 October 2014

Thermo-optic coefficient of electrochemically etched porous silicon layer was measured through temperature-dependent reflectance spectroscopy subjected to temperatures ranging from 302.15K to 594.15K. Porous silicon was fabricated via electrochemical etching of a p-type (100) silicon wafer in an ethanol – HF solution with applied current densities of 2.5mA/cm², 5mA/cm² and 15mA/cm² to form ~2µm thick pSi layers. Using Cauchy's dispersion equation and Bruggeman's effective medium approximation, refractive index and porosity of the samples were calculated respectively. A Fabry-Perot filter derived from the pSi single layers was also fabricated. Normal incidence reflectance spectroscopy was utilized to characterize the filter at different temperatures. The behavior of light in the multilayered structure under different temperatures was modeled using Transfer Matrix Method. The results show that the experimental data is in good agreement with the simulation model. From the empirical data and the simulation results, optical tuning of the Fabry-Perot filter through temperature can be done.

Keywords: Porous silicon, Thin film, Electrochemical etching, Thermo-optic effect, Thermo-optic coefficient, Fabry-Perot filter, Thermo-optical tuning.

1. INTRODUCTION

Porous silicon (pSi) is a sponge-like structure of hydrogen – covered silicon (Si) [1]. It is formed through electrochemical etching of crystalline Si in an ethanoic HF solution [1 and 2]. Porous silicon is an interesting material for semiconductor device fabrication due to its visible luminescence [3], large surface area [1 and 4], and tunable refractive index as a function of depth [2]. In addition, the fabrication cost is cheap and the set – up can easily be done at room temperature.

In the electrochemical etching process of Si, some of the fabrication parameters considered are the electrolyte concentration; supplied anodic current; and etching time. Average pore sizes of the pSi produced is strongly dependent on the electrolyte concentration. The thickness of pSi layer is controllable with etching time. Furthermore, porosity of pSi is directly proportional on the supplied anodic current. Varying the supplied current results to porosity variation and consequently, refractive index tunability is possible [1].

Due to the tunable refractive index property of pSi, it can be fabricated into multilayered structures such as anti-reflection coatings (ARC) [2], distributed Bragg reflectors (DBR) [5 and 6], and Fabry-Perot (FP) filters [6]. However, the refractive index of pSi is not constant with temperature [7 and 8]. Since the wavelength dependence of these passive optical devices scales with the refractive index, their operation varies at each given temperature. The phenomenon at which refractive index varies with temperature is known as the thermo-optic effect (TOE) [9]. The Thermo-optic effect is significant in the fabrication of optoelectronic devices such as optical switching, filter and laser tuning, and sensing applications [10 and 11]. One way to quantify the TOE is through the measurement of the thermo-optic coefficient (TOC) of a material. The thermo-optic coefficient is simply the change of refractive index as a function of temperature [11].

This paper presents temperature-dependent reflectance of pSi with different porosities. Thermo-optic coefficients were calculated from the reflectance data and were used to obtain an empirical fit for FP filter fabrication. An FP filter was chosen because it reflects a long range of wavelength while allowing transmission only at a certain wavelength. With this mechanism, optical tuning is possible.

Derived from the single layer pSi samples, an FP filter was fabricated and was subjected to temperature-dependent reflectance spectroscopy. To model the light propagation in the multilayered FP filter, the transfer matrix method (TMM) from *Saplagio et. al* [12] was used. The empirical data was in good agreement with the simulation fit. With these results, thermo - optical tuning of an FP filter based on pSi can be done.

2. METHODOLOGY

Boron doped crystalline Si (100) substrates, with resistivity 0.007-0.025 $\Omega\cdot\text{cm}$, were cut into dimensions of 1cm x 1.75cm. The substrates underwent standard degreasing procedure to remove grease and unwanted particles on their surface. These were then dried using pressurized high purity nitrogen gas. Substrates were then subjected to electrochemical etching in a lateral anodization cell set – up. Figure 1 shows the schematic diagram of the anodization cell, where the Si substrate served as the anode and a silver plate as the cathode. The electrolyte used in the anodization cell was composed of 12% HF with equal parts of ethanol. Anodic current was supplied using a Tektronix PWS4721 Programmable DC power supply.

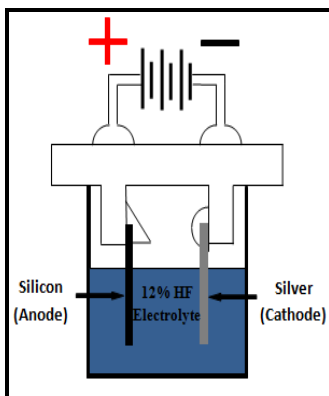


Figure 1. Schematic diagram of lateral anodization cell set - up used for the Si electrochemical etching.

Three single layer pSi films were fabricated and the etching parameters for each sample are summarized in Table 1. The porous layers were fabricated each to have a thickness of 2µm. For the FP filter fabrication, etching parameters are shown in Table 2. The filter was tuned to 540nm. It was composed of 2 DBR's with pSi2 as the optical cavity in between. Each DBR is composed of alternating periodic layers of pSi1 and pSi3 by varying the etching current density with time. This structure satisfies the Bragg condition given by Equation 1 where λ_0 , n , and d are the central wavelength, refractive index, and thickness of the given porous layer, respectively. The calibration parameters used for the single layers and FP filter fabrication are based on calibration experiments presented in this journal: [13].

$$\frac{\lambda_0}{4} = nd \tag{1}$$

Table 1. Etching parameters used for single layer pSi fabrication.

Sample	Etching current density (mA/cm ²)	Etch time (sec)
pSi1	2.5	1000.2
pSi2	5	625.2
pSi3	15	277.8

Table 2. Etching parameters used for the fabrication of pSi - based FP filter tuned to 540nm.

Layer	Etching current density (mA/cm ²)	Etch time (sec)
n1	5	20
n2	2.5	45
spacer	15	43

For pore investigation and cross-sectional measurement, samples were characterized via scanning electron microscopy using a Philips XL30 FESEM. Optical characterization was done via temperature – dependent reflectance spectroscopy. Shown in Figure 2 is a schematic diagram of the temperature – dependent reflectance spectroscopy set – up. The sample was mounted on a thermal stage subjected to different temperature which ranges from 303.15K – 594.15K. Optical reflectance was done using a SPEX 500 monochromator installed with 600 grooves/mm grating. The broadband light source used was a 100W OSRAM tungsten – halogen lamp with Si photodiode as the detector. The temperature setting of the thermal stage was allowed to stabilize first before reflectance measurements were done.

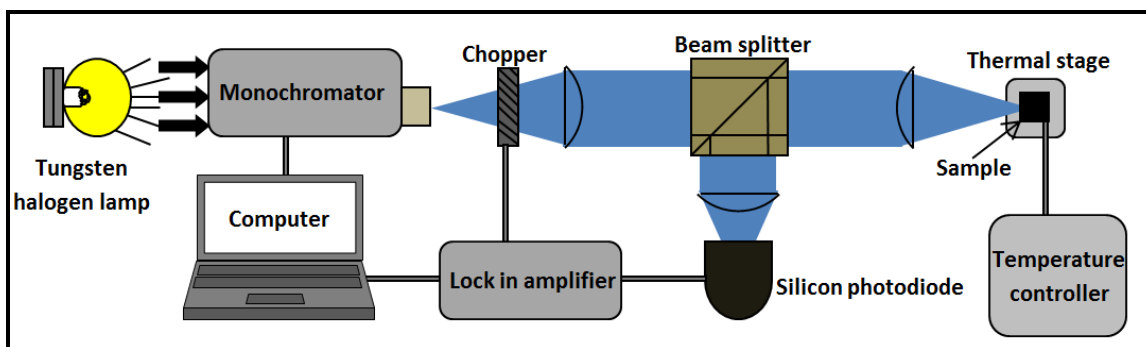


Figure 2. Schematic diagram of temperature-dependent reflectance spectroscopy set-up.

From the reflectance spectra of the samples at each given temperature, the refractive index was calculated using Cauchy’s dispersion equation [14]. The calculated refractive index of the samples subjected to room temperature was used to calculate the porosities using Bruggeman effective medium approximation [15].

3. RESULTS AND DISCUSSION

3.1. Single layer pSi

Shown in Figure 3 are top view SEM images of pSi samples pSi1, pSi2, and pSi3. The presence of pores on the Si matrix can be observed from the samples' surface. Shown in Figure 4 are the cross-sectional SEM images of the samples. From these micrographs, pore depth is considered as the effective thickness of pSi. In this case, the fabricated pSi layers were measured to be ~2µm thick, same as intended film thickness. For the optical characterization of the samples, normal incidence temperature – dependent reflectance spectroscopy was performed. From the measured thicknesses and reflectance spectra of the samples, refractive indices were computed using Equation 2 [16]:

$$2nd \left(\frac{1}{\lambda_r} - \frac{1}{\lambda_{r+1}} \right) = 0 \tag{2}$$

where d is the effective thickness of the layer and λ_r is the wavelength of the r th extrema (shown in Figure 5).

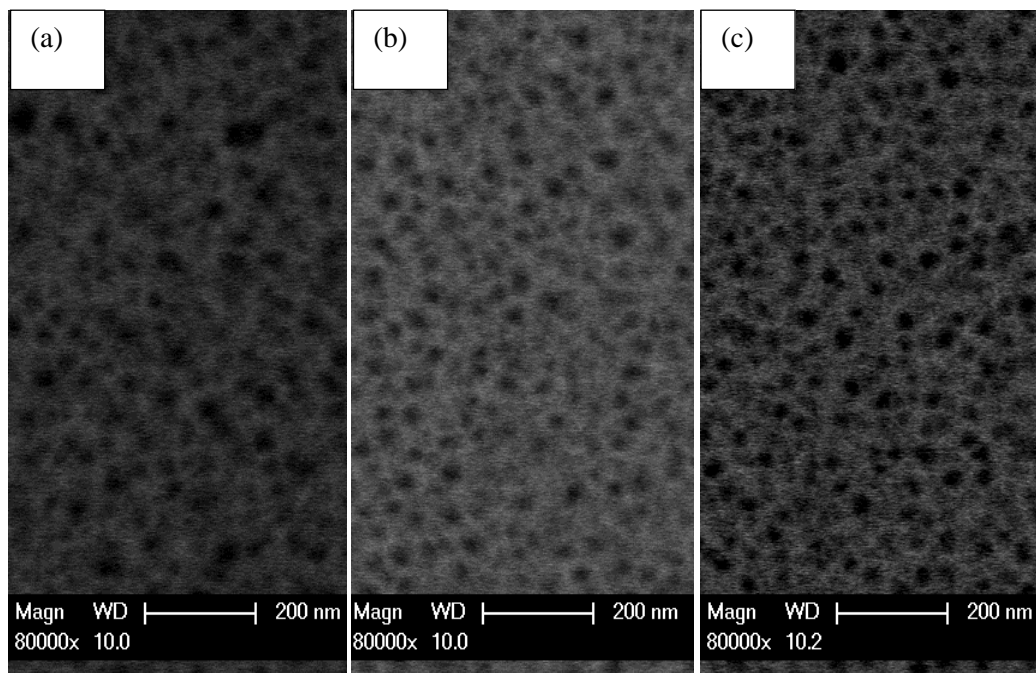


Figure 3. SEM images of the single layer pSi: (a) pSi1, (b) pSi2, and (c) pSi3.

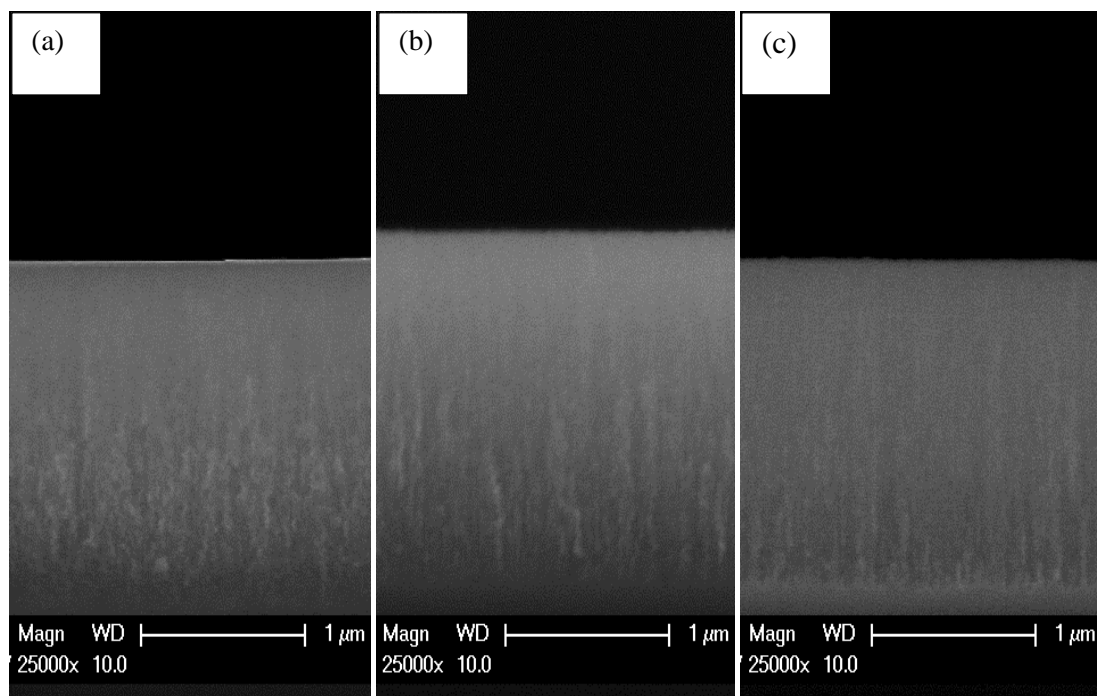


Figure 4. Cross - sectional SEM images of the single layer pSi: (a) pSi1, (b) pSi2, and (c) pSi3.

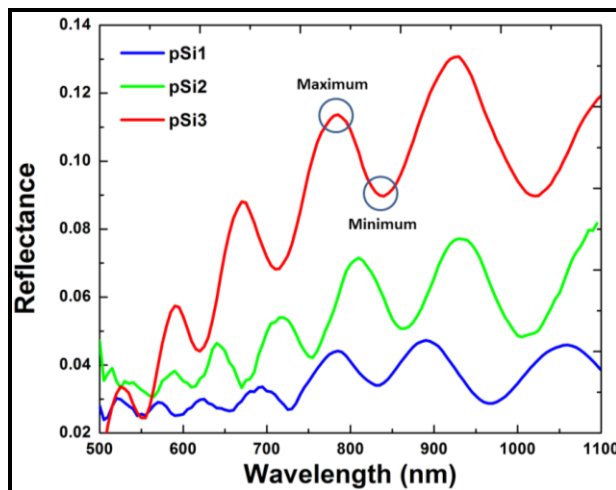


Figure 5. Room temperature reflectance spectra of the samples showing the extrema of the single layer pSi samples.

To characterize each sample according to their porosity, the computed refractive index of the samples when subjected to room temperature was used in the Bruggeman's effective medium approximation (equation 3) [15 and 17]:

$$p \frac{n_{air}^2 - n_{pSi}^2}{n_{air}^2 + 2n_{pSi}^2} + (1 - p) \frac{n_{Si}^2 - n_{pSi}^2}{n_{Si}^2 + 2n_{pSi}^2} = 0 \tag{3}$$

where n_{pSi} , n_{Si} , and n_{air} are the refractive indices of the pSi, Si, and air respectively. Values of n_{Si} and n_{air} are given in references [18] and [19] respectively. Calculated porosities of the pSi samples are shown in Table 3. It can be seen that samples etched at higher current densities result to higher porosities. This linear relation between current density and porosity agrees with the result of [20]. Moreover, it can be stated that the porosity is inversely proportional to the refractive index. This is because the pore volume of the pSi layer is relatively reduced with decreasing porosity, and vice versa.

Table 3. Calculated porosities of the pSi samples computed using the Bruggeman effective medium approximation

Sample	Current density (mA/cm ²)	Porosity (%)
pSi1	2.5	58.72
pSi2	5	67.29
pSi3	15	76.79

Figure 6 shows the reflectance spectra of pSi1 and its corresponding refractive index when it was subjected to different temperatures. From Figure 6a, it can be noted that oscillations are present. This is due to the presence of pSi layer which is considered to be a homogeneous layer or a thin film [21]. Shifting of the reflectance spectra with respect to temperature can also be noticed. As stated

before, this is because n_{pSi} varies with different temperature and is shown in Figure 6b. To compute for the TOC of the samples, the refractive index of each sample was plotted as a function of temperature. Measurement of the TOC of the pSi samples were done by linear regression analysis of the temperature – refractive index curve given in Figure 7 [22].

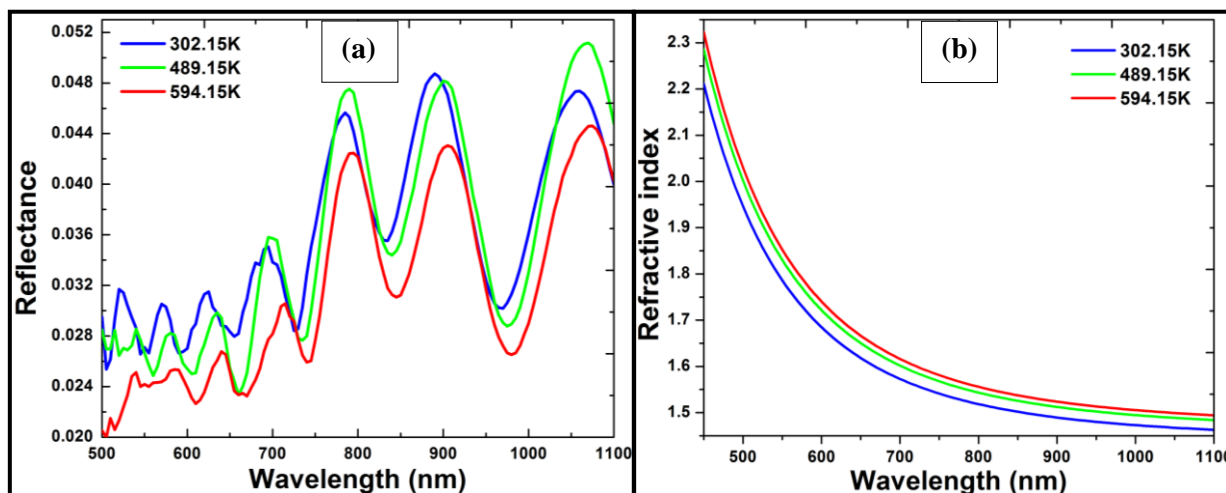


Figure 6. Temperature-dependent (a) reflectance spectra and (b) refractive index dispersion of pSi1. The reflectance spectra show a shifting to longer wavelengths and values of refractive index are increasing with higher temperature.

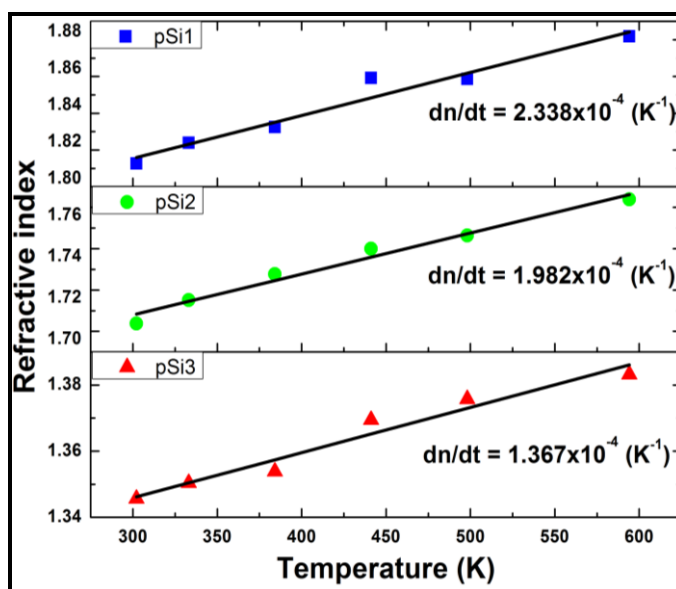


Figure 7. Temperature - refractive index curve of pSi sample showing the TOC at 540nm. The curves show a linear relation.

Figure 8 shows the TOC of each pSi with respect to the wavelength of the light incident to the sample. It can be seen that the TOC of pSi is still dispersive, as in crystalline Si [23]. In addition, with

increasing porosity of pSi, a decrease in the values of the TOC was observed. This is because TOC is inversely related to porosity which is consistent with the results of *Moretti et. al* [8].

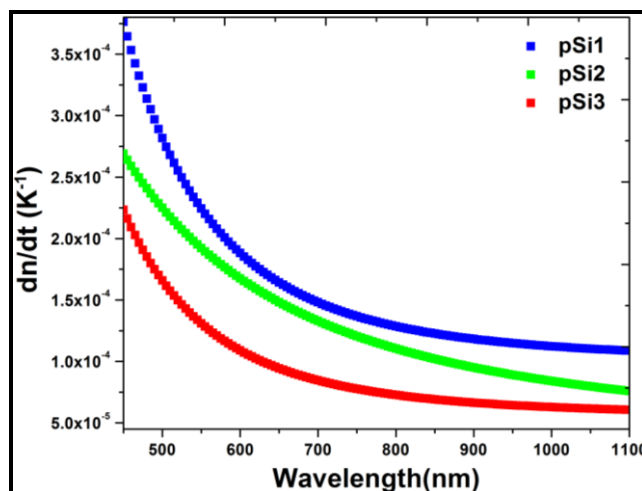


Figure 8. Experimental data showing the TOC dispersion of the pSi samples with different porosities: pSi1, $p = 58.72\%$; pSi2, $p = 67.29\%$; and pSi3, $p = 76.79\%$.

3.2 Multilayer

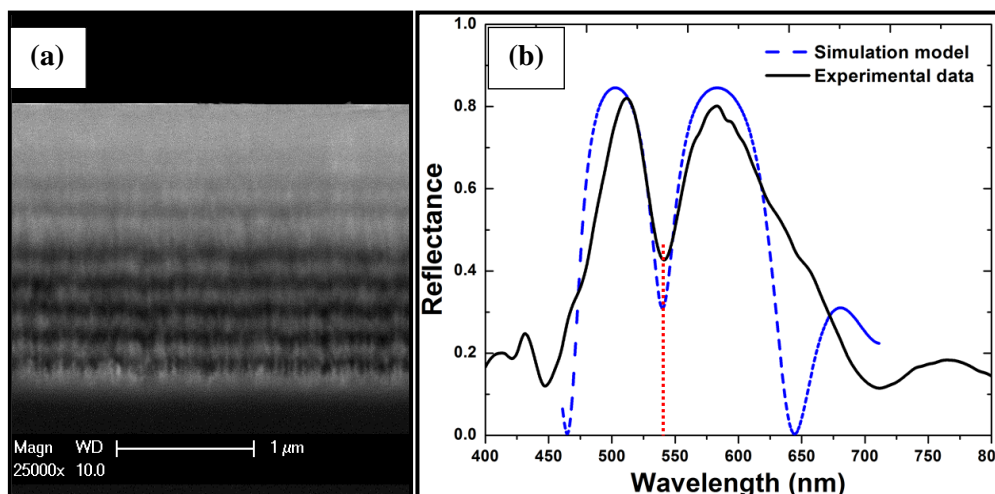


Figure 9. (a) Cross-section SEM image and (b) room temperature reflectance spectra with TMM simulation of the fabricated FP filter. The dotted line in the reflectance spectra indicates the optical cavity which is tuned to 540nm.

Shown in Figure 9a is the SEM image of the FP filter. An alternating bright and dark layer signifies the presence of pSi with different porosities, and the thick layer in the middle is the spacer which serves as the optical cavity. The bright layers in the image correspond to the layers with relatively lower porosity (p_l) and dark layers with higher porosity (p_h). This is because the p_l layers is relatively denser than the p_h layers. Beside the structure observation, optical reflectance of FP filter

was investigated and is shown in Figure 9b together with its simulation model. Transfer Matrix Method was used to model the behavior of light in the FP filter. However, the experimental result does not perfectly fit with the model due to the identical losses which could be attributed to the change in thickness and refractive index in each of the layers of the FP filter [24].

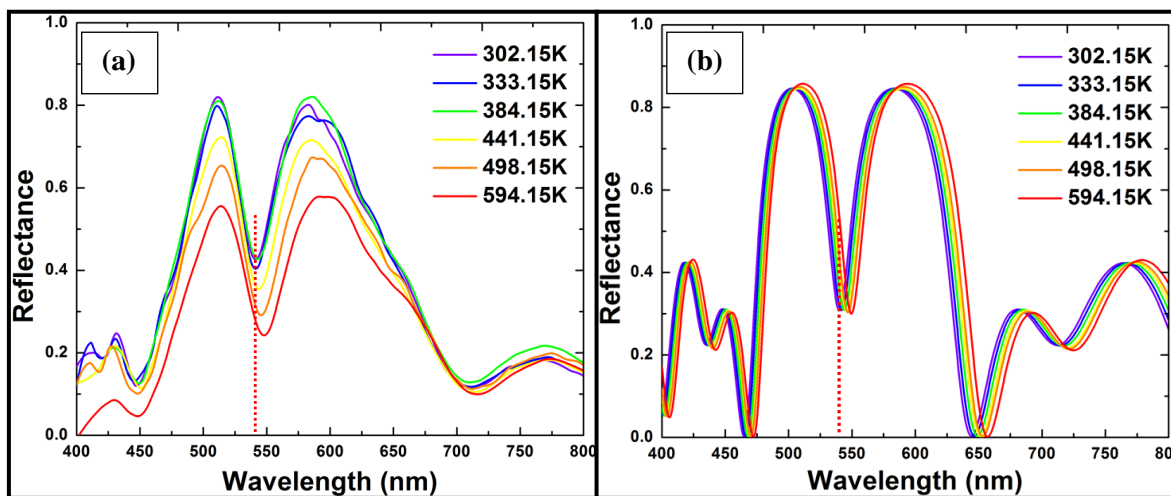


Figure 10. (a) Reflectance spectra of the FP filter subjected to temperature–dependent reflectance spectroscopy and (b) the TMM simulation model. The dotted line shows the optical cavity of the filter at room temperature.

In Figure 10, reflectance spectra of the FP filter at different temperature and its corresponding simulation were reported. It can be noted that both the experimental data and simulation model shift to longer wavelengths. This wavelength shifting is due to the thermal variation of refractive index of the FP filter. The redshift can be explained by the relation given in Equation 1 where the wavelength is a function of the refractive index [25]. As the samples' temperature increases, refractive index also increases which results to the shifting of the reflectance to longer wavelengths. A drop in the reflectance intensity of the filter with respect to temperature was also observed which is due to the increase in absorption of the FP filter as the temperature increases.

4. CONCLUSION

Thermo–optic coefficient of electrochemically etched porous silicon was calculated through temperature–dependent reflectance spectroscopy. Refractive index and porosity were measured using Cauchy's empirical equation and Bruggemann's effective medium approximation respectively. Fabrication of FP filter based on the single layer pSi was successfully done. The FP filter was also subjected to temperature–dependent reflectance spectroscopy. A redshift of the reflectance of the filter was observed which is due to the thermal variation of the refractive index. A drop of the reflectance intensity of the FP filter at increasing temperature was also observed and was attributed to the increase

in absorption of pSi at higher temperature. Simulation model of FP filter based on TMM does not perfectly fit with the experimental result due to which could be attributed to the change in thickness and refractive index in each of the layers of the FP filter. However, the experimental data is in good agreement with the simulation model. With the empirical and simulation data, thermo – optical tuning of a pSi-based FP filter can be done.

ACKNOWLEDGEMENTS

The authors would like to acknowledge the National Research Council of the Philippines (NRCP), Philippine Council for Industry and Energy Research and Development (PCIERD), Department of Science and Technology Grants-in-Aid (DOST-GIA) Program, University of the Philippines Office of the Vice-Chancellor for Research and Development (UP-OVCRD) and Accelerated Science and Technology Human Resource Development Program (ASTHRDP) for their support

References

1. V. Torres-Costa, RJ. Martin-Palma. *Journal of Material Science* 45(11) (2010) 2823-2838.
2. JH. Selj, A. Thøgersen, SE. Foss, ES. Marstein. *Journal of Applied Physics*, 107(7), (2010) 074904.
3. Q. Ma, R. Xiong, MY Huang. *Journal of Luminescence* 131(10) (2011) 2053-2057
4. S.Sam, L. Touahir, J. Salvador Andresa, P. Allongue, JN. Chazalviel, AC. Gouget-Laemmel, S. Djebbar. *Langmuir* 26(2) (2009) 809-814.
5. S. Um, SG. Lee, HG. Woo, S. Cho, H. Sohn. *Journal of nanoscience and nanotechnology* 13(1) (2013) 288-293.
6. M. Kolle, B. Zheng, N. Gibbons, JJ Baumberg. *Optics Express* 18(5) (2010) 4356-4364
7. K. Nishida, M. Fujii, S. Hayashi, J. Diener. *Applied Physics Letters* 96(24) (2010) 243102-243102.
8. L. Moretti, L. De Stefano, A. Rossi, I. Rendina. *Applied Physics Letters* 86(6) (2005) 061107.
9. M. Deen, P. Basu. *Silicon Photonics: Fundamentals and Devices*. John Wiley & Sons, West Sussex (2012)
10. N. Rouger, L. Chrostowski, R. Vafaei. *Journal of Lightwave Technology* 28(9) (2010) 1380-1391
11. L. Vivien, L. Pavesi. *Handbook of Silicon Photonics*, CRC Press, New York (2013)
12. N. Saplagio, A. Mabilangan, M. Faustino, L. Lopez Jr., A. Somintac, A. Salvador. *Int. J. Electrochem. Sci.*, 9 (2014): To be published.
13. A. Mabilangan, N Saplagio, E. Anguluan, N. Cabello, R. Gonzales, A. Somintac, A. Salvador. *Science Diliman*. 25 (2013) 15-28
14. KS. Pérez, JO. Estevez, A. Méndez-Blas, J. Arriaga, G. Palestino, ME. Mora-Ramos. *Nanoscale research letters* 7(1) (2012) 1-8
15. VH. Pham, H. Bui, LH. Hoang, TV. Nguyen, TS. Pham, QM. Ngo. *Journal of the Optical Society of Korea* 17(5) (2013) 423-427.
16. D. Schroder, *Semiconductor Material and Device Characterization*. John Wiley & Sons, New Jersey (2006)
17. J. Peckham, GT Andrews. *Thin Solid Films* 520(7) (2012) 2526-2531
18. M. Brass, G. Li, EV. Stryland, *Handbook of Optics, 3rd edition, Vol. 4*. McGraw-Hill, New York (2009)
19. T. Yoshizawa. *Handbook of Optical Metrology: Principle and Applications*, CRC Press, New York (2009)
20. P. Kumar, P. Huber, *Journal of Nanomaterials* 2 (2007) 89718-89722.
21. AY. Panarin, SN. Terekhov, KI. Kholostov, VP. Bondarenko. *Applied Surface Science* 256(23) (2010) 6969-6976.

22. S. Wiechman, J. Müller. *Thin Solid Films*, 517(24) (2009) 6847-6849.
23. A. Alexandridis, E. Chondrodima, K. Moutzouris, D. Triantis. *Journal of Materials Science*, 47(2) (2012) 883-891.
24. UC. Hasar, IY. Ozbek, EA. Oral, T. Karacali, H. Efeoglu. *Optics Express* 20(20) (2012) 22208-22223.
25. D. Hohlfeld, M. Epmeier, H. Zappe. *Sensors and Actuators A: Physical* 103(1) (2003) 93-99.

© 2014 The Authors. Published by ESG (www.electrochemsci.org). This article is an open access article distributed under the terms and conditions of the Creative Commons Attribution license (<http://creativecommons.org/licenses/by/4.0/>).